A direct charge pumping technique for spatial profiling of hot-carrier induced interface and oxide traps in MOSFETs

S. Mahapatra [a,*], C.D. Parikh [a], J. Vasi [a], V. Ramgopal Rao [b], C.R. Viswanathan [b]

[a] *Department of Electrical Engineering, Indian Institute of Technology, Bombay, India*
[b] *Department of Electrical Engineering, University of California, Los Angeles, CA, USA*

Received 13 July 1998

Abstract

A new charge pumping (CP) technique is proposed to obtain the spatial profile of interface-state density (N_{it}) and oxide charges (N_{ot}) near the drain junction of hot-carrier stressed MOSFETs. Complete separation of N_{it} from N_{ot} is achieved by using a direct noniterative method. The pre-stress CP edge is corrected for the charges associated with both the generated N_{it} and N_{ot}. A closed form model is developed to predict the stress-induced incremental CP current. The damage distributions are obtained after fitting the model with experimental data.

1. Introduction

Hot-carrier degradation is a long-term MOSFET reliability issue [1]. The degradation results from localized buildup of interface states (N_{it}) and oxide charges (N_{ot}) near the drain junction during hot-carrier stressing [2]. To understand and model the degradation, different charge pumping (CP) based methods have been employed to obtain the spatial profiles of both N_{it} and N_{ot} [3–8]. In all these methods, the CP current is measured while the CP area is varied. This is followed by a differential analysis, which, along with information about the CP edge, furnishes the N_{it} profile. The changes in the local surface potential after degradation furnish the N_{ot} profile. To obtain accurate damage distributions, the issues that need attention are (i) accurate determination of the CP edge in the unstressed device, (ii) correction of the pre-stress CP edge to account for charges in the generated interface states and oxide traps and (iii) separation of the N_{it} and N_{ot} created during stress.

In the existing reverse-bias methods, an ac waveform form [3] or a dc bias [4] is applied to the source and drain junctions to vary the effective CP area. The CP edge is determined from computer simulations. However, these methods suffer from the gate induced drain leakage (GIDL) problem at larger reverse biases. In the semi-direct method [5], the effective CP area is changed by applying a pulse train of varying amplitude at the gate. The CP edge is determined from the pre-stress characteristics, with the help of back-up computer simulations to predict the maximum CP area. These simulation-based techniques [3–5] are unsatisfactory since they require precise knowledge of the device structure and doping profiles (which are neither always available nor easily determinable). The direct methods [6–8] overcome this problem, where again the effective CP area is varied by applying a pulse train of varying amplitude at the gate. However, now the CP edge is determined from the pre-stress characteristics measured on transistors having different drawn gate lengths, and

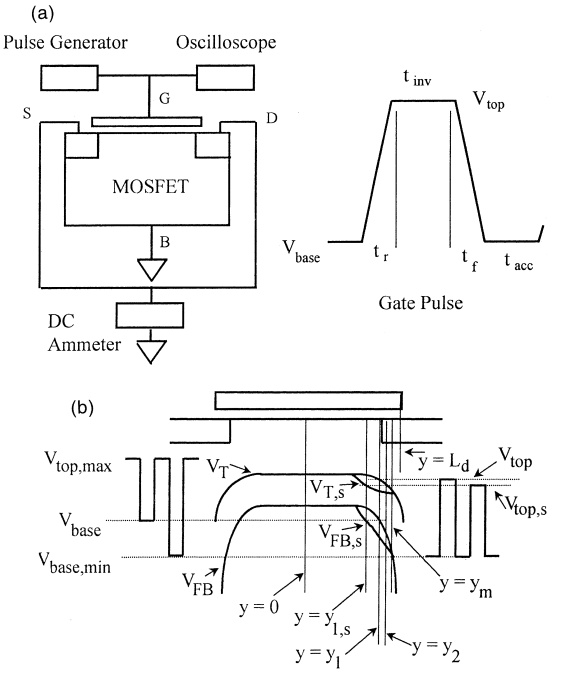

Fig. 1. (a) Charge pumping setup and applied gate waveform. (b) Typical threshold and flatband voltage distributions before (V_T, V_{FB}) and after ($V_{T,s}$, $V_{FB,s}$) stressing. The charge pumping edges are related to the top and base level of the gate pulse as $V_{FB}(y_1) = V_{base}$, $V_T(y_1) = V_{top}$, $V_{FB}(y_m) = V_{base,max}$, $V_{FB,s}(y_{1,s}) = V_{base}$, $V_{T,s}(y_{1,s}) = V_{top,s}$ and $V_T(y_2) = V_{top,s}$.

does not require computer simulations [9]. The correction to the pre-stress CP edge and the separation of N_{it} from N_{ot} are performed either by neutralization of N_{ot} by a brief carrier injection of the opposite type [6,7], or by an iterative correction scheme [8].

However, as shown recently [10], the increased CP current with larger gate pulse amplitude is not only due to the increased CP area, but also due to the increased energy zone of recombination in the band gap, and the possible nonuniformity of interface-state density, energetically in the band gap and spatially near the junction. The conventional approach [9] does not take these effects into account and thus furnishes an incorrect CP edge. Therefore, the direct methods [6–8], being based on [9], yield an incorrect damage profile [10]. Moreover, the intermediate carrier injection techniques [6,7] need separate experimental tools to monitor complete N_{ot} neutralization, and hence in general are complex in nature. On the other hand, the iterative scheme [8], being dependent on repetitive differentiation of experimental data, is highly susceptible to measurement noise and may give rise to convergence problems.

In this paper, the CP edge in the pre-stress case is determined using the new approach [10], which does not suffer from the inconsistency associated with the conventional schemes [9]. This approach has now been modified as follows. The pre-stress CP edge is corrected for the additional charges associated with both N_{ot} and N_{it} generated due to stress. By employing both the varying pulse-top and varying pulse-base CP schemes [3], N_{it} is completely separated from N_{ot} without using the iterative approach [8]. A closed-form model, having two independent parameters is formulated to predict the stress-induced incremental CP current. The model is fitted with experimental data, and the optimized parameter values are used to determine the damage profiles. The method, being immune to measurement noise (since numerical differentiation of the experimental data is avoided), provides accurate distributions of both N_{it} and N_{ot} created during stress.

In Section 2, the new technique along with the CP current model is proposed. Results obtained from the technique are discussed in Section 3, followed by conclusions in Section 4.

2. Theory

In charge pumping, the gate of the MOSFET is pulsed from accumulation to inversion using a trapezoidal waveform. The substrate is shorted to ground. The de current arising out of electron–hole recombination at the interface states is measured at the source and drain, as shown in Fig. 1(a).

Fixing the pulse top in inversion (at $V_{top,max}$) and varying the pulse base (V_{base}) level, the charge pumping current (I_{cp}) from an unstressed symmetric transistor is given by [3]

$$I_{cp}(V_{base}) = qfW\int_{-y_1}^{y_1} N_{it}(y)\mathrm{d}y, \tag{1a}$$

where q is the electronic charge, f is the frequency of the gate pulse, W is the width of the transistor and $N_{it}(y)$ is the pre-stress interface-state density at y. The edge of the charge pumping zone y, is defined by $V_{FB}(y_1) = V_{base}$ (see Fig. 1(b)), where $V_{FB}(y)$ is the local flatband voltage [11]. The origin is chosen at the center of the channel. Similarly, by fixing the pulse base in accumulation (at $V_{base,min}$) and varying the pulse top (V_{top}) level, the charge pumping current is given by [3]

$$I_{cp}(V_{top}) = qfW\left[\int_{-y_m}^{-y_1} N_{it}(y)\mathrm{d}y + \int_{y_1}^{y_m} N_{it}(y)\mathrm{d}y\right], \tag{1b}$$

where the edges of the charge pumping zone are defined by $V_T(y_1) = V_{top}$ and $V_{FB}(y_m) = V_{base,min}$ (see Fig. 1(b)).

In a stressed transistor, interface states are created

and charges are trapped in regions close to the drain junction. The presence of charges in the interface states and oxide traps change the local V_T and V_{FB} distributions near the drain junction. Therefore, the varying V_{base} and varying V_{top} post-stress charge pumping currents ($I_{cp,s}$) are given by

$$I_{cp,s}(V_{base}) = qfW\left[\int_{-y_1}^{0} N_{it}(y)dy + \int_{0}^{y_{1,s}} N_{it,s}(y)dy\right] \quad (2a)$$

and

$$I_{cp,s}(V_{top,s}) = qfW\left[\int_{-y_m}^{-y_2} N_{it}(y)dy + \int_{y_{1,s}}^{y_m} N_{it,s}(y)dy\right], \quad (2b)$$

where $N_{it,s}(y)$ is the post-stress interface-state density along the channel and the new (stressed) charge pumping edge $y_{1,s}$ is given by $V_{FB,s}(y_{1,s}) = V_{base}$, where $V_{FB}(y)$ is the post-stress local flatband voltage distribution in the drain half of the channel (see Fig. 1(b)). Similarly, the post-stress local threshold voltage distribution is $V_{T,s}$ and the edge $y_{1,s}$ will correspond to a new pulse top level defined by $V_{T,s}(y_{1,s}) = V_{top,s}$. The unstressed charge pumping edge corresponding to $V_{top,s}$ is y_2 and is defined by $V_T(y_2) = V_{top,s}$ (see Fig. 1(b)). We have assumed in writing Eq. (2b) that $V_{FB,s}(y_m) = V_{FB}(y_m) = V_{base,min}$, which is valid since for y_m deep inside the junction, the N_{it} and N_{ot} generated at y_m are not significant to make any appreciable change in the V_{FB} distribution.

The increase in base-level charge pumping current due to interface-state generation is given by

$$\Delta I_{cp}(V_{base}) = I_{cp,s}(V_{base}) - I_{cp}(V_{base}) \simeq qfW\int_{0}^{y_{1,s}} \Delta N_{it}(y)dy, \quad (3)$$

where $\Delta N_{it}(y)$ is the generated interface-state density. We have assumed in writing Eq. (3) that $\int_0^{y_{1,s}} \Delta N_{it}(y)dy \gg \int_{y_1}^{y_{1,s}} N_{it}(y)dy$, which is valid since for a given V_{base} value, $y_{1,s} \gg |y_{1,s} - y_1|$, and for significant damage creation (for which $y_{1,s}$ can be different from y_1), $\Delta N_{it}(y) \gg N_{it}(y)$ at any y. Similarly, the incremental top-level charge current is given by

$$\Delta I_{cp}(V_{top,s}) = I_{cp,s}(V_{top,s}) - I_{cp}(V_{top,s}) \simeq qfW\int_{y_{1,s}}^{y_m} \Delta N_{it}(y)dy, \quad (4)$$

where we have assumed like before that $\int_{y_{1,s}}^{y_m} \Delta N_{it}(y)dy \gg \int_{y_2}^{y_{1,s}} N_{it}(y)dy$. Note that Eqs. (3) and (4) satisfy the relation

$$\Delta I_{cp}(V_{top,s}) + \Delta I_{cp}(V_{base}) = \Delta I_{cp,max}(V_{top,max}, V_{base,min}) = qfW\int_{0}^{y_m} \Delta N_{it}(y)dy, \quad (5)$$

so that for a given value of V_{base} and hence ΔI_{cp} in post-stress, the corresponding value $V_{top,s}$ can be obtained from Eq. (5). We will come to this later in this section.

Now, at any point y along the channel, the post-stress local V_T and V_{FB} values are related to the pre-stress ones by [3]

$$V_{T,s}(y) = V_T(y) - \frac{q\Delta N_{ot}(y)}{C_{ox}} + \frac{q\Delta N_{it}(y)}{2C_{ox}} \quad (6)$$

and

$$V_{FB,s}(y) = V_{FB}(y) - \frac{q\Delta N_{ot}(y)}{C_{ox}} - \frac{q\Delta N_{it}(y)}{2C_{ox}}, \quad (7)$$

where C_{ox} is the oxide capacitance per unit area. In writing Eqs. (6) and (7), we have assumed that the interface states are created uniformly over the band gap, the states in the upper half of the band gap are acceptor-like and those in the lower half are donor-like [3]. Note that in the post-stress case, $V_{T,s}(y_{1,s}) = V_{top,s}$ and $V_{FB,s}(y_{1,s}) = V_{base}$. So, by subtracting Eq. (7) from Eq. (6), the effect of oxide trap charges are removed and for a given $y_{1,s}$ along the channel, we obtain

$$V_{top,s} - V_{base} = V_T(y_{1,s}) - V_{FB}(y_{1,s}) + \frac{q\Delta N_{it}(y_{1,s})}{C_{ox}}. \quad (8)$$

As discussed earlier, for a given V_{base} and hence ΔI_{cp} in post-stress, the corresponding $V_{top,s}$ can be obtained from Eq. (5). The pre-stress $V_T(y)-y$ and $V_{FB}(y)-y$ relations can be obtained from the $I_{cp}-V_{base}$ and $I_{cp}-V_{top}$ measurements (performed on identical transistors having different gate lengths) as discussed later. The $y_{1,s}-V_{base}$ relation can be found from Eq. (3) by constructing an empirical model for ΔN_{it} having adjustable parameters to relate ΔI_{cp} with V_{base}. Finally, Eq. (8) is optimized for the parameter values, and the damage distribution is obtained with the final set of parameters, as discussed in the remaining part of this section.

We now describe the model to predict incremental base-level charge pumping current. Note that for MOSFETs with thin gate oxides, the hot-carrier induced interface states are highly localized and their distribution follows the lateral electric field distribution along the channel [12]. The lateral field and hence the damage distribution can be modelled best as

Gaussians. However, gaussians are not amenable to analytical modeling, especially integration. An earlier paper on modeling the charge pumping current used a box distribution for interface-state density [13]. In this paper, we model the interface-state density profile by an analytically integrable function close to the Gaussian in shape as

$$\Delta N_{it}(y) = \frac{N_{it,p}}{\cosh^2 \alpha (y - y_p)}, \tag{9}$$

where $N_{it,p}$ is the peak value of damage, y_p is the position of the peak along the channel and α is a parameter whose reciprocal is a measure of the spatial spread of the damage. Substituting Eq. (9) into Eq. (3) one obtains

$$\Delta I_{cp}(V_{base}) = qfW \frac{N_{it,p}}{\alpha}[1 + \tanh \alpha (y_{1,s} - y_p)], \tag{10}$$

and for the maximum incremental charge pumping current

$$\Delta I_{cp,max}(V_{top,max}, V_{base,min}) = qfW \frac{N_{it,p}}{\alpha}[1 + \beta], \tag{11}$$

where it is assumed that $\tanh \alpha y_p = 1$, whose physical implication is that the contribution to the total incremental charge pumping current by the interface-states generated in the source half of the channel is negligible. In Eq. (11), β is defined by the relation

$$\beta = \tanh \alpha (y_m - y_p), \tag{12}$$

where β, along with α, determines the position of the damage peak along the channel.

Now, using Eqs. (10) and (11) one obtains, after some simple manipulations,

$$y_{1,s} = y_m - \frac{1}{2\alpha} \ln \left[\frac{2 - (1 + \beta)x}{(1 - \beta)x} \right], \tag{13}$$

where $x = \Delta I_{cp}/\Delta I_{cp,max}$. Finally, using Eqs. (12) and (13) in Eq. (9) and putting all together in Eq. (8), one obtains

$$V_{top} - V_{base} = f_{VTFB}(y_{1,s}) + \frac{4q\alpha \Delta I_{cp,max}}{qfWC_{ox}(1 + \beta)} \frac{1}{G},$$

$$G = \frac{(1 + \beta)x}{2 - (1 + \beta)x} + \frac{2 - (1 + \beta)x}{(1 + \beta)x} + 2, \tag{14}$$

where f_{VTFB} is a second order polynomial fitted through the pre-stress V_T-V_{FB} versus y data, and $y_{1,s}$ is given by Eq. (13). Eq. (14) is fitted with the experimental ($V_{top} - V_{base}$) versus $\Delta I_{cp}/\Delta I_{cp,max}$ data and the two unknown parameters, namely α and β are obtained.

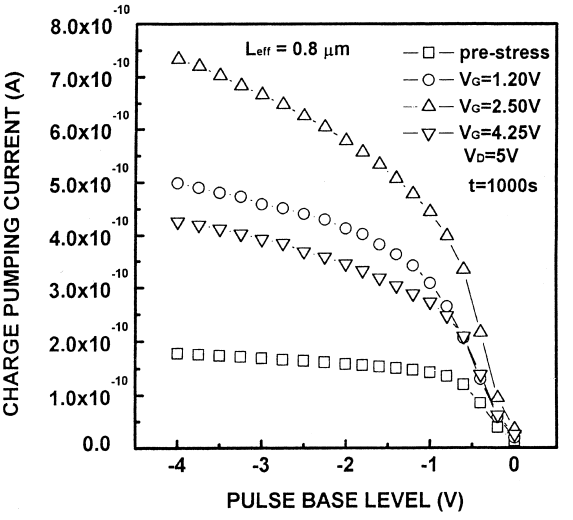

Fig. 2. Pre- and post-stress charge pumping current versus pulse base level. The pulse frequency was 1 MHz and the top level was held at 1 V. The stressings were done at $V_G = 1.2$, 2.5 and 4.25 V, $V_D = 5$ V for $t = 1000$ s.

The damage parameters $N_{it,p}$ and y_p are then obtained from Eqs. (11) and (12).

Once the parameters α and β are obtained, for each of the V_{base} (and hence ΔI_{cp}) values in post-stress, the charge pumping edge $y_{1,s}$ is obtained from Eq. (13). Since $V_{FB,s}(y_{1,s}) = V_{base}$ at $y_{1,s}$, $V_{FB,s}$ is known. Again, from the pre-stress V_{FB}–y relation, for $y_{1,s}$. V_{FB} is also known. So, from Eq. (7), ΔN_{ot} can be obtained, since the ΔN_{it} values are already obtained from Eq. (9).

Now, to obtain the V_{FB}–y relation in pre-stress, Eq. (1a) can be rewritten as [10]

$$\frac{I_{cp}(V_{base})}{2qfW} = \langle N_{it}(V_{base}) \rangle \left[\frac{L_d}{2} - \Delta y_1(V_{base}) \right], \tag{15}$$

where $\langle N_{it}(V_{base}) \rangle$ is the spatial average of $N_{it}(y)$ upto y_1. Δy_1 is the zone excluded from charge pumping and is related to the charge pumping edge y_1 by $y_1(V_{base}) = L_d/2 - \Delta y_1(V_{base})$, L_d being the drawn gate length. While $y_1(V_{base})$ is dependent on the drawn gate length, $\Delta y_1(V_{base})$ is not. $I_{cp}(V_{base})$, measured on transistors of different L_d but identical otherwise, is plotted as a function of $L_d/2$. The data points are fitted with a straight line. The intercept of the fitted straight line gives Δy_1 and hence y_1 [10]. This process is repeated for all V_{base} values to obtain y_1 as a function of V_{base}, which is essentially the pre-stress V_{FB}-y relation. In a similar manner, the pre-stress $\frac{1}{2}(I_{cp}(V_{base,max}) - I_{cp}(V_{top}))$ data is plotted versus $L_d/2$. The intercepts of the fitted straight lines through the data points drawn for all V_{top} values furnishes the V_T–y relation as before.

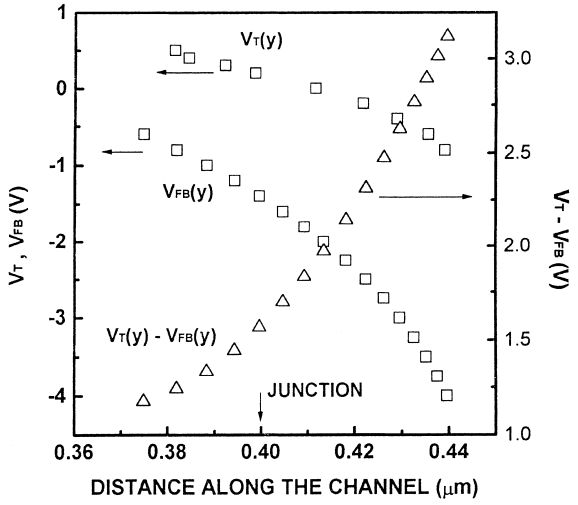

Fig. 3. Pre-stress V_T, V_{FB} (left y-axis) and $V_T - V_{FB}$ (right y-axis) distribution along the channel.

3. Results and discussion

The charge pumping setup is shown in Fig. 1(a). The gate of the MOSFET is pulsed using a trapezoidal waveform obtained from an HP33120A function generator. The charge pumping current is measured at the source and drain using a Keithley 617 electrometer, preceeded by an LC low-pass filter. The substrate is shorted to ground. Measurements were performed using gate pulses having a frequency of 1 MHz with rise and fall time of 250 ns. Both the varying base level and the varying top level charge pumping schemes were employed. Experiments were performed using isolated LDD n-channel MOSFETs having 1.0 to 0.4 μm drawn (0.8 to 0.2 μm effective) channel lengths, oxide thickness of 110 Å and gate width of 10 μm. In the present paper, the stress-induced damage profiles are shown only for the device having 1.0 μm drawn channel length in order to establish the new technique. The detailed data will be presented elsewhere.

In Fig. 2, pre- and post-stress charge pumping currents are plotted as a function of pulse base level. The pulse top was held at 1 V. Stressing was done at $V_D = 5$ V for 1000 s. The gate voltages chosen during stressing were 1.2, 2.5 and 4.25 V. Note that for each gate bias, stress experiments were done on different devices but with the same channel length. The increase in charge pumping current after stress is due to interface-state generation. The post-stress charge pumping current is maximum for $V_G = 2.5$ V, minimum for

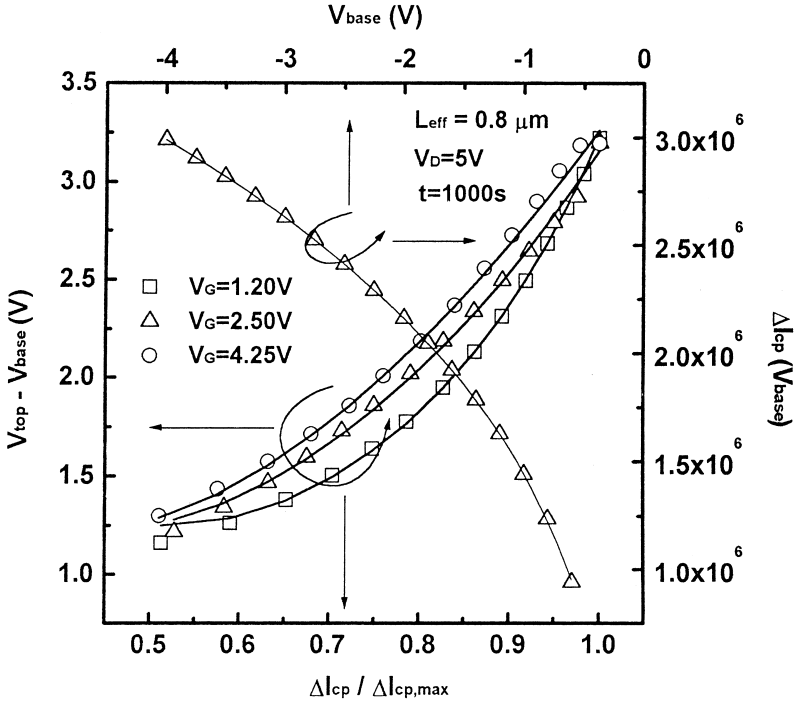

Fig. 4. Calculated (solid line) and experimental (symbols) $V_{top} - V_{base}$ versus $\Delta I_{cp}/\Delta I_{cp,max}$ plot (left y- and bottom x-axis). The stressings were done at $V_G = 1.2$, 2.5 and 4.25 V, $V_D = 5$ V for $t = 1000$ s. Also shown are the calculated and experimental $\Delta I_{cp}/V_{base}$ plot (right y, top x axis) for the $V_G = 2.5$ V case.

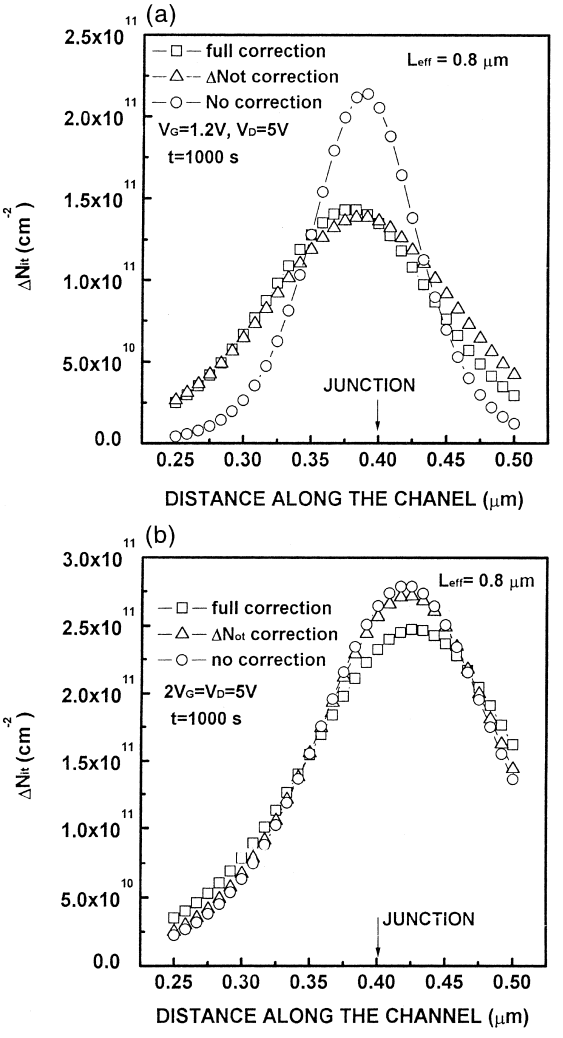

Fig. 5. Calculated ΔN_{it} profiles alone the channel without correction, with correction for only oxide charges and with full correction (both oxide and interface charges) for (a) $V_G = 1.2$ V and (b) $V_G = 2.5$ V stress condition. The stress V_D was 5 V for t = 1000 s.

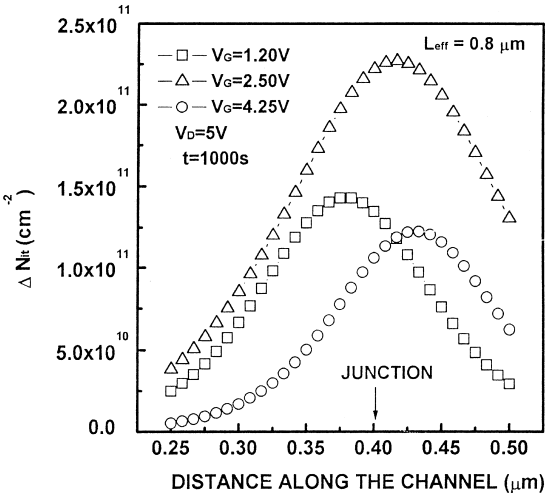

Fig. 6. ΔN_{it} profiles along the channel. The stressings were done at $V_G = 1.2$, 2.5 and 4.25 V, $V_D = 5$ V for $t = 1000$ s.

$V_G = 4.25$ V, while the $V_G = 1.2$ V curve falls in between the two. This implies that maximum interface-state generation takes place for the $V_G = V_D/2$ stress condition, which also happens to be the bias for maximum substrate current I_{sub} recorded during stress.

In Fig. 3, the pre-stress V_T and V_{FB} distributions are plotted along the channel (left y-axis). These relations are obtained from the $I_{cp}-V_{top}$ and $I_{cp}-V_{base}$ measurements performed on transistors having different drawn gate lengths as described in the previous section. Also shown (right y axis) is the pre-stress V_T-V_{FB} relation along the channel. The V_T and V_{FB} distributions will change after stress due to charges associated with both ΔN_{it} and ΔN_{ot}. However, the V_T-V_{FB} distribution will change only due to charges associated with ΔN_{it} (see Eqs. (6) and (7)). Thus the effect of charges associated with ΔN_{ot} can be removed.

In Fig. 4, $V_{top}-V_{base}$ is plotted as a function of $\Delta I_{cp}/\Delta I_{cp,max}$ (left y axis and bottom x axis). Stressing was performed for 1000 s at $V_D = 5.0$ V. The gate voltages were 1.2. 2.5 and 4.25 V. The symbols are experimental data points, and the solid lines are the model fit, as obtained from Eq. (14). As can be seen the model fits the experimental data extremely well. The model parameters α and β are extracted from such fits, performed for all stress conditions. To estimate the quality of the fits, the $\Delta I_{cp}-V_{base}$ relation was reconstructed from Eq. (10) with the extracted parameters and is shown (solid lines) along with the data points (right y axis and top x-axis) for the $V_G = 2.5$ V case. As can be seen, the calculated values again fit the experimental data extremely well.

In Fig. 5a and b, the generated interface-state density as a function of position are shown for stress at $V_G = 1.2$ V and 2.5 V respectively. The stress V_D was 5 V for $t = 1000$ s. The effect of corrections due to the presence of interface and oxide charges on the interface-state density profiles are also shown. For the $V_G = 1.2$ V case (Fig. 5a), there is significant hole trapping. So, the profile obtained after correction for ΔN_{ot} only is significantly different from the uncorrected one. However, since there are not many charges in the interface states, not much improvement is observed when corrected further for these additional interface charges (full correction). In the $V_G = 2.5$ V case (Fig. 5b), there is no significant oxide charge trapping. So, the profile obtained after correction for ΔN_{ot} only is not significantly different from the uncorrected one. When further correction is performed for the interface

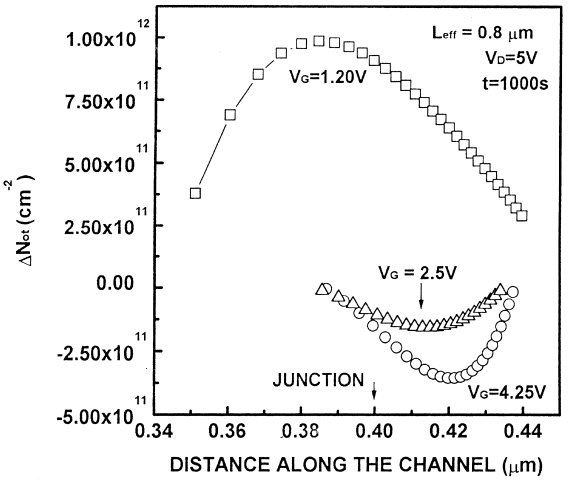

Fig. 7. ΔN_{ot} profiles along the channel. The stressings were done at $V_G = 1.2$. 2.5 and 4.25 V, $V_D = 5$ V for $t = 1000$ s.

charge, a significant change in the profile is observed, since in this condition, the interface-state generation is significant.

In Fig. 6, the interface-state density profiles are plotted along the channel. The stressing was done at $V_D = 5$ V for 1000 s. The gate voltages were chosen to be 1.2, 2.5 and 4.25 V. The maximum interface states are produced for $V_G = 2.5$ V, consistent with maximum incremental charge pumping current. The damage spread is also maximum in this condition. This is expected because for the $V_G = V_D/2$ stress condition, maximum impact ionization followed by injection of both electrons and holes in large numbers into the oxide takes place. For the other two stress conditions, either fewer electrons or holes are injected and hence both the damage magnitude and spread is less. For $V_G = 1.2$ V, the damage takes place closer to the channel, while for the other two cases, the peak damage occurs closer to the gate edge. This is consistent with the movement of the pinch-off region towards the junction with increasing V_G during stress.

In Fig. 7, the calculated oxide trapped charges are plotted along the channel. The stress V_G were 1.2, 2.5 and 4.25 V, for 1000 s. The stress V_D was 5 V. Hole trapping is observed at $V_G = 1.2$ V case, while electron trapping is observed at $V_G = 2.5$ and 4.25 V, as expected. For the $V_G = V_D/2$ stress condition, fewer trapped charges are observed than the other two cases. The hole trapping at low V_G takes place away from the junction into the channel region, while the electron trapping at high V_G takes place inside the junction. This is again consistent with the movement of the pinch-off region. In our devices, we observe more hole trapping than electron trapping. The reason can be attributed to low mobility of holes in the oxide and transverse field assisted detrapping of electrons from the oxide traps.

Similar data with consistent trends have been obtained for transistors of different channel lengths, stressed at a variety of gate and drain voltages for different times. This attests to the reliability and robustness of the proposed technique.

4. Conclusion

To summarize, a new robust charge pumping (CP) technique is proposed to obtain the spatial profile of interface-state density (N_{it}) and oxide trapped charge (N_{ot}) near the drain junction of hot-carrier stressed MOSFETs. The CP edge in the pre-stress case is uniquely determined using a reliable method which is free from the inconsistency associated with the conventional approach. The post-stress CP edge is obtained by correcting the pre-stress one for the additional charges associated with both N_{ot} and N_{it} generated due to stress. A direct noniterative scheme is utilized to completely separate N_{it} from N_{ot}. Numerical differentiation of the experimental data is avoided by formulating a model for the stress-induced incremental CP current. The model is fitted with the experimental data, and the extracted parameter values are used to determine the damage profiles.

Acknowledgements

SM would like to acknowledge Siemens AG, Germany for providing a research fellowship.

References

[1] Hu C, Tam SC, Hsu FC, Chan TY, Terill KW. IEEE Trans. Electron Devices 1985;32:375.
[2] Heremans P, Bellens R, Groeseneken G, Maes HE. IEEE Trans. Electron Devices 1998;35:2194.
[3] Chen W, Balasinski AQ, Ma TP. IEEE Trans. Electron Devices 1993;40:187.
[4] Li HH, Chu YL, Wu CY. IEEE Trans. Electron Devices 1997;44:782.
[5] Lee RGH, Su JS, Chung SS. IEEE Trans. Electron Devices 1996;43:81.
[6] Chen C, Ma TP. In: Symposium on VLSI Technology, Digest of Technical Papers, 1996. p. 230 IEEE Cat. No. 96CH35944.
[7] Ang DS, Ling CH. IEEE Electron Device Lett. 1998;19:23.
[8] Chim WK, Leang SE, Chan DSH. J. Appl. Phys. 1997;81:1992.
[9] Tsuchiaki M, Hara H, Morimoto T, Iwai H. IEEE Trans. Electron Devices 1993;40:1768.

[10] Mahapatra S, Parikh CD, Vasi J, IEEE Trans. Electron Devices [accepted].
[11] Groeseneken G, Maes HE, Beltran N, Keermaecker RF. IEEE Trans. Electron Devices 1984;31:42.
[12] Ancona MG, Saks NS, McCarthy D. IEEE Trans. Electron Devices 1988;37:2221.
[13] Lee RGH, Wu JP, Chung SS. IEEE Trans. Electron Devices 1996;43:898.